The Transient Response of Organic Electrochemical Transistors

*Pushpa R. Paudel Michael Skowrons Drona Dahal Raj Kishen Radha Krishnan Björn Lüssem**

P. R. Paudel, M. Skowrons, D. Dahal, R. K. Radha Krishnan, Prof. B. Lüssem
Department of Physics
Kent State University
Kent, Ohio 44242, USA
Email Address: blussem@kent.edu
Prof. B. Lüssem
Institut for Microsensors, Microactuators, and Microsystems (IMSAS)
University of Bremen
Bremen, Germany
Phone: +49 (0421) 218 62610
Email Address: bluessem@imsas.uni-bremen.de

Keywords: *Organic Electrochemical Transistors, Drift-Diffusion Modeling, Transient Model*

A fast response of Organic Electrochemical Transistors (OECTs) to electrical or chemical changes is essential for a widespread acceptance of this technology. However, finding design rules for fast switching OECTs is complicated by the fact that current transient device models are highly simplified and rely on a one dimensional approximation of the device that neglects details of the ion and hole concentration inside the transistor channel.
To improve our understanding of transient processes limiting the speed of OECTs, a two-dimensional drift diffusion model is presented and experimentally validated. It is shown that switching is strongly influenced by lateral ion currents that were neglected in previous models. A consistent treatment of these currents leads to a dependency of the time constants on the applied drain potential and a complex dependency of the response time constants on the detailed device geometry.
In addition to an improved understanding of the transient response of OECTs, the results discussed here highlight the challenges in properly characterizing switching time constants of OECTs, and reinforce the necessity to ensure that switching is measured between two steady-state conditions, and not between transient states.

1 Introduction

Organic Electrochemical Transistors (OECTs) take advantage of a strong coupling between ion and electron transport observed in some polymeric semiconductors[1]. Their high performance[2] facilitates sensing very small fluctuations in electrical potential at the gate electrode, which was used e.g. to monitor brain activity[3]. Furthermore, functional coatings applied to the gate electrode make OECTs selective to small chemical changes, which can be used to design highly sensitive (bio-)sensors[4, 5, 6, 7]. Combined with their mechanical flexibility, stretchability[8], and self-healing properties[9, 10], OECTs have become a key technology for (organic) bioelectronics[11].
A fast response to electric and chemical changes is essential for organic biosensors. When used to sense and amplify neuronal activity[2], a temporal resolution in the $1 - 10\ ms$ range is desirable. Changes in neurotransmitter concentration occur at similar timescales, but longer time changes (range of several minutes) are of interest as well e.g. when studying processes such as neuromodulation[12].
Recent results show that OECTs are well equipped to reach this benchmark. For example, OECTs using various channel materials, electrolytes, or fabrication techniques reached time constants below $1\ ms$.[13, 14, 15, 16, 17, 18, 19, 20, 21, 22, 23, 24]. Although most of these OECTs rely on the doped p-type semiconductor PEDOT:PSS[13, 14, 15, 16, 17, 18, 19], other materials such as P3CPT,[20] p(g2T-TT)[21, 22], and diketopyrrolopyrrole (DPP)-based donor-acceptor (D–A) polymers such as P(lgDPP-MeOT2) and P(bgDPP-MeOT2)[23] reach a high performance as well. Table 1 summarizes the switching speeds of OECTs reported in literature.
Response times were found to vary proportional to the time constant of the electrolyte circuit represented by a series connection of the ionic resistance of the electrolyte and the gate capacitance. This time constant is influenced by the geometry of the device, and it was shown that limiting the overlap between the channel and the source/drain contacts, the OECT channel length and the thickness of the organic semiconductor improve the speed of OECTs greatly. [17, 25, 24, 26]

Table 1: Summary of reported OECT switching speeds

Channel	Electrolyte	Time constants (τ)	Ref.
PEDOT:PSS	Polymer Electrolyte‡ [30]	$\tau_{on,off} = 0.9, 0.03\ s$	[13]
PEDOT:PSS	PBS	$\sim 0.1\ ms$	[14]
PEDOT:PSS	NaCl	$39\ \mu s$	[2]
PEDOT:PSS	Solid electrolyte‡ [30]	$\tau_{on,off} \approx 30, 5\ ms$	[27]
PEDOT:PSS	PBS	$\sim 1.5\ ms$	[16]
PEDOT:PSS	NaCl	$0.03 - 1.2\ ms$	[17]
P3CPT	$H_2O : OH^- + H_3O^+$	$\sim 10^1\ s$	[20]
PEDOT:PSS	NaCl	$\geq\ 1s$	[31]
PEDOT:PSS	CTAB†	$\geq\ 1s$	[32]
PEDOT:PSS	NaCl	$\sim 1\ s$	[18]
PEDOT:PSS	H_2O	$\sim\ 10\ s$	[18]
PEDOT:PSS	Solid electrolyte‡ [30]	$\tau_{on,off} \approx 3.3,\ 0.4\ s$	[19]
p(g2T-TT)	NaCl	$0.1 - 1\ ms$	[21]
p(g2T-TT)	NaCl	$0.1\ ms$	[22]
p(a2T-TT)	NaCl	$1.2\ ms$	[22]
P(lgDPP-MeOT2)	NaCl	$\tau_{on,off} = 578, 63\ \mu s$	[23]
P(bgDPP-MeOT2)	NaCl	$\tau_{on,off} = 516, 30\ \mu s$	[23]
PEDOT:PSS/TX	poly(vinyl alcohol)	$\tau_{on,off} \approx 33, 6\ ms$	[9]
PEDOT:PSS	Internal ion-gated Gated ⋆	$2.6\ \mu s$	[28]
PEDOT:PSS - PEI	Internal ion-gated Gated⋆	$2.9\ \mu s$	[29]

‡51 wt.% DI water, 33 wt.% PSSNa, 8 wt.% D-sorbitol, & 8 wt.% glycerol (85 wt.%)

†Cetyltrimethylammonium bromide

⋆PEDOT:PSS channel hydrated with D-sorbitol and salt solution without a separate electrolyte part.

The time constant can be reduced further by optimizing the materials parameters of the electrolyte. For example, OECTs utilizing halide based liquid electrolytes were shown to reach a performance which is sufficient for medical applications, such as recording of ECG signals.[14, 15, 16] Relatively slower OECTs, with a response time in the millisecond regime, use viscous and solidified electrolytes,[27] or poly(vinylalcohol) hydrogels.[9] Internal ion-gated OECTs having ion-reservoirs embedded inside channel itself are shown to attain speeds of few microseconds in response to low gate signals.[28, 29] Aside from the type of electrolyte, its concentration affects the speed of OECTs as well, and in particular a very low concentration influences the speed negatively.[20, 18]

The transient response of OECTs was shown to be composed of initial fast ($< 1s$) response followed by slow change, which occurs over a longer timescale ($\sim\ 1s$)[20]. A higher concentration of electrolytes reduces the influence of the slower response.[18, 20]. Finally, several reports show that the speed of OECTs depend on the mobility of ions inside the channel and the ease with which ions move in and out the channel.[21, 22, 23] The ionic mobility depends on the amount of hydration of the channel and an optimum hydration enhances conductivity of ions.[21, 22] Furthermore, the presence of taylored side chain and moieties of the organic semiconductor facilitates a more efficient ion injection/ejection in the polymer bulk.[23]

Despite these promising results, it is challenging to formulate clear design rules for fast OECTs. Several transient device models were proposed that address this shortcoming[33]. Most of these models build on a transient and steady-state model proposed by Bernards et al.[34] in 2007. The general setup of these models is sketched in **Figure 1**. Assuming that the OECT is a p-type depletion transistor e.g. consisting of the organic semiconductor PEDOT:PSS, a positive voltage applied to the gate electrode leads to an injection of cations into the organic semiconductor. In Bernards model, this process is modeled by a capacitance C_G. Denoting the ion concentration and electric potential along the transistor channel by $p_{ion}(x)$ and $\phi(x)$, this capacitance C_G is defined as (V_{GS}: voltage applied to the gate electrode)

$$C_G = \frac{e p_{ion}(x)}{V_{GS} - \phi(x)}. \tag{1}$$

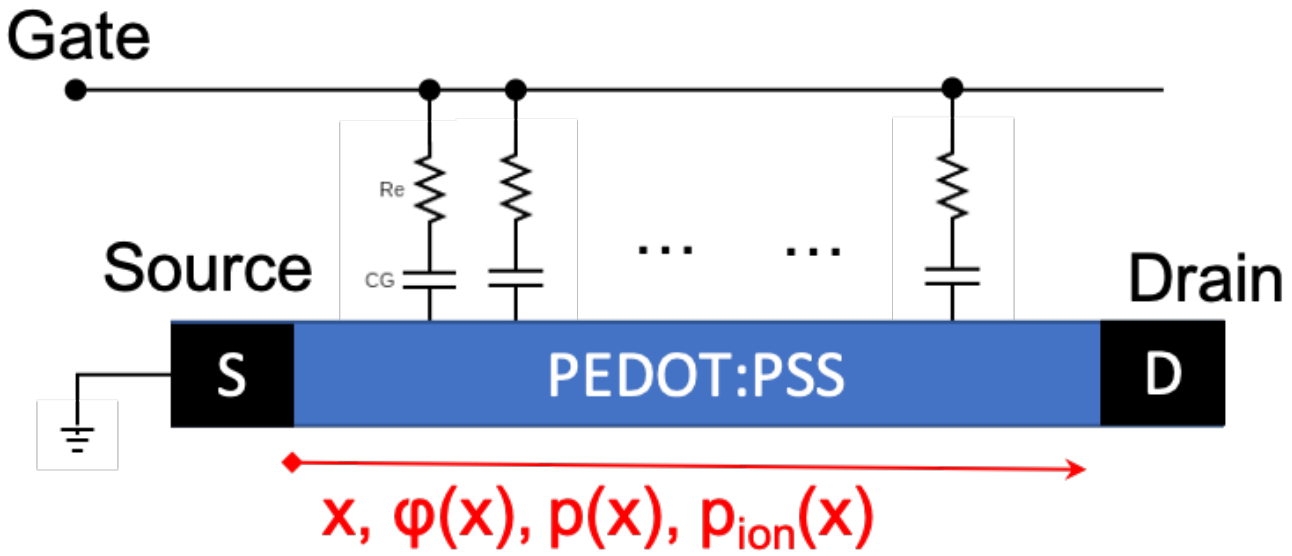

Figure 1: Setup of Bernards model. Coupling between hole and ion transport is described by a gate capacitance C_G defined as the ratio of injected cations to applied voltage. Furthermore, the ionic resistance of the electrolyte R_e is included in the model.

In Equation 1, it is assumed that the gate capacitance scales with the volume of the organic semiconductor, which is indeed observed in experiments[17].
Injection of cations leads to de-doping of the organic semiconductor and hence modulation of the density of free holes. It is assumed that every cation replaces one mobile hole. Assuming that the organic semiconductor (e.g. PEDOT:PSS) is initially doped at a concentration p_0, one obtains

$$p(x) = p_0 - p_{ion}(x). \tag{2}$$

Under these assumptions the potential along the transistor channel at steady state conditions becomes[35] (L: channel length, $V_P = \frac{ep_0}{C_G}$: pinch off voltage, e: elementary charge)

$$\Phi(x) = (V_{GS} - V_P) + \sqrt{\left[V_{DS} - (V_{GS} - V_P)\right]^2 \frac{x}{L} - (V_P - V_{GS})^2 \left(\frac{x}{L} - 1\right)}, \tag{3}$$

and finally, the steady-state drain current $I_{D,ss}$ in dependence of the gate and drain potential V_{GS} and V_{DS} reads as ($G = e\mu p_0 \frac{wT}{L}$ conductance of the organic semiconductor at $V_{GS} = V_{DS} = 0$, w, T, L: width, thickness, and length of the transistor channel, μ: hole mobility)

$$I_{D,ss} = G\left(1 - \frac{V_{GS} - \frac{V_{DS}}{2}}{V_{PO}}\right) V_{DS} \tag{4}$$

Equations 3 and 4 are valid in the steady state only and further approximations have to be taken to derive an analytical solution for the transient problem. For example, Bernards et al.[34] proposed to average the hole and ion concentration along the transistor channel, e.g. to use $\overline{p}(t) = \frac{1}{L}\int_0^L p(x,t)dx$ and $\overline{p_{ion}}(t) = \frac{1}{L}\int_0^L p_{ion}(x,t)dx$ instead of the full distribution $p(x,t)$ and $p_{ion}(x,t)$. With this approximation, it is possible to reduce the complexity of the problem to one (the vertical) dimension. The drain current density j becomes[34]

$$j = e\left(\mu\overline{p}(t)\frac{V_{DS}}{L} + fL\frac{d\overline{p}(t)}{dt}\right) \tag{5}$$

$$= e\left(\mu\overline{p}(t)\frac{V_{DS}}{L} - fL\frac{d\overline{p_{ion}}(t)}{dt}\right) \tag{6}$$

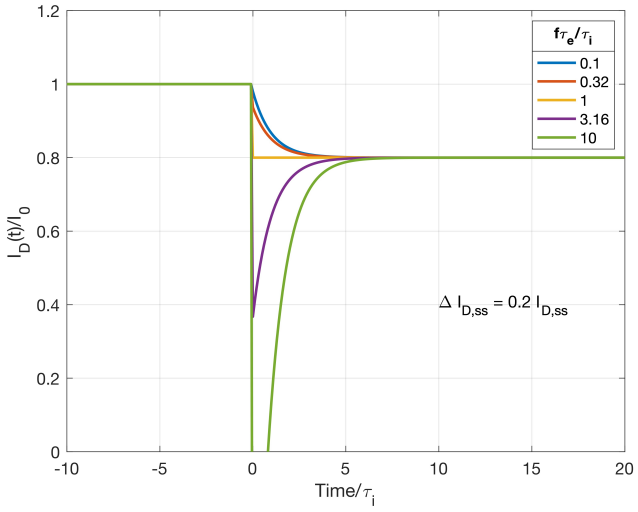

Figure 2: Response of an OECT to a voltage step applied at the gate electrode as predicted by the model of Bernards et al.[34]. The characteristic of the response depends on the ratio of electronic to ionic time constant τ_e/τ_i. For small ratios, a gradual relaxation is observed, which changes into a spiking response for increasing τ_e. In both cases, the exponential decrease is described by the ionic time constant τ_i.

Here, f is an experimental factor that was added to account for the error introduced by the averaging process.
Assuming that the device is operated in the linear regime (e.g. $V_{DS} < V_{GS}$), Bernards et al. arrived at the following transient drain current in response to a voltage step from $0V$ to ΔV_{GS} applied to the gate electrode:

$$I_D(t, V_{GS}) = I_{D,ss} + \Delta I_{D,ss}\left(\Delta V_{GS}\right)\left(1 - f\frac{\tau_e}{\tau_i}\right)\exp\left(-\frac{t}{\tau_i}\right) \tag{7}$$

Here $\Delta I_{D,ss} = I_0 - I_{D,ss}\left(\Delta V_{GS}\right)$ and $I_0 = I_{D,ss,lin}(V_{GS} = 0) = GV_{DS}$. Equation 7 shows that the response is defined by two time constants. The first one, $\tau_e = \frac{L^2}{\mu V_{DS}}$, can be identified as the electronic time constant of the system, i.e. the characteristic time for a hole to traverse through the whole channel. The second time constant, $\tau_i = C_G R_s$ (R_s: ionic resistance of the electrolyte, cf. Figure 1), represents the time constant of the ionic system. τ_i can be interpreted as the characteristic time for charging the ionic capacitance described by Eq. 1.
Equation 7 shows that the response of OECTs to a voltage pulse can be categorized into two different regimes, depending on the ratio of $f\frac{\tau_e}{\tau_i}$ (cf. **Figure 2**). When $\tau_e \ll \tau_i$, the system slowly relaxes toward the new steady-state. If, however, $\tau_e \approx \tau_i$, i.e. for longer channel lengths or low charge mobility in the organic semiconductor, the transient current spikes first before slowly relaxing toward the new steady state. In both cases, however, the characteristic time constant describing the exponential relaxation is determined by the ionic time constant τ_i.
Several authors proposed improvements to this original model[36, 37, 38, 39, 40]. In most instances, a more precise definition of the correction factor f is sought. For example, Faria et al. defined f as the ratio of gate currents flowing to the drain electrode over the total gate currents[36, 37]. Similarly, Friedlein et al. attempted to include a simplified spatial dependence of the gate current by modeling the coupling between gate and source and between gate and drain differently[38].
The interpretation of the correction factor f was complicated further by a recent result of Kaphle et al.[35], who argued that the steady state distribution of ions and holes and the potential distribution along the transistor channel are influenced by lateral migration of ions - an effect not included in the original model of Bernards et al.. As a result, the potential along the transistor channel is found to deviate strongly from Eq. 3. Furthermore, considering that the channel length of OECTs is usually several orders of magnitude larger than the thickness of the semiconductor, lateral ion currents will react much slower than vertical ones, and the precise distribution of ions and holes along the transistor chan-

nel, thus far only approximated by the ad-hoc factor f, will become essential to understand the transient behavior of OECTs.
Here, we address this lack in our understanding of the response of OECTs to changing input signals. We use our two-dimensional drift-diffusion model of OECTs and extend it to be able to model the transient processes. For the first time, we are able to study the transient response of OECTs without ad-hoc assumptions about the ion and hole distribution along the transistor channel. It is shown that the transient response is marked by two distinct time constants - a short time constant describing the movement of ions perpendicular to the transistor channel and a second, longer one describing the flow of lateral ion currents along the channel to reach the equilibrium of the device. Whereas the perpendicular injection of ions already leads to a complete on and off switching of the device, the steady-state of the device is only reached after all lateral currents have subsided. Measurements of the transient response of OECTs faster than the lateral time constant leads to a frequency, geometry, and drain potential dependent response, complicating the interpretation of transient OECT measurements.

2 Results and Discussion

2.1 Model

To study the response of OECTs to an arbitrary voltage signal, Poisson's and Continuity Equations of holes p and Cations p_{ion} are solved self-consistently using the Gummel Scheme in two dimensions (ϵ: permittivity, ϕ: electric potential, C: immobile charge, e.g. dopants, $\vec{j}_p, \vec{j}_{ion}$: hole and cation current density, x, y: horizontal and vertical coordinate, respectively)

$$\nabla\epsilon\nabla\phi(x,y) - e\left(C(x,y) - p(x,y) - p_{ion}(x,y)\right) = 0 \tag{8}$$

$$\nabla\vec{j}_{ion}(x,y) - \frac{\partial p_{ion}(x,y)}{\partial t} = 0 \tag{9}$$

$$\nabla\vec{j}_{p}(x,y) - \frac{\partial p(x,y)}{\partial t} = 0 \tag{10}$$

Setting the time derivatives $\frac{\partial}{\partial t}$ in Eqs. 9 and 10 to zero results in the steady-state solution[35, 41]. Similarly, reducing the ion current to $\vec{j}_{ion}(x,y) \equiv j_{ion,y}(x)\vec{e}_y$, the hole current to $\vec{j}_p(x,y) \equiv j_{p,x}(x)\vec{e}_x$, and the hole and cation concentrations to $p_{ion}(x,y) \equiv p_{ion}(x)$ and $p(x,y) \equiv p(x)$ would recover the original (steady state) model proposed by Bernards et al.[34].
Here, the full system of Eqs. 8-10 is solved to study the transient response without having to approximate the electric potential, hole, and cation concentration by an average value $\overline{\phi}, \overline{p}, \overline{p_{ion}}$. The time dependence imposed by the time derivatives $\frac{\partial p}{\partial t}, \frac{\partial p_{ion}}{\partial t}$ is calculated using an Euler scheme, and care has been taken to choose time steps small enough to limit the overall error. The results are checked by comparing the transient currents for long times to the steady-state solution of the device.
The geometry of the OECTs is shown in **Figure 3**. The device consists of a layer of the electrolyte, in which the hole concentration is set to zero, and a layer of the organic semiconductor. The doping concentration p_0 is kept fixed inside the organic semiconductor, and both, holes and cations are treated as mobile. Throughout the device, the anion concentration is assumed to be constant, i.e. movement of anions is not considered.
The two layers are contacted by the source electrode on the lower left, the drain electrode on the lower right, and the gate electrode on the top. The width of the gate electrode on top is varied; for the results discussed in Secs. 2.2-2.4.1, the electrode covers the whole length of the device, whereas it is assumed to only cover the middle part of the device for Sec. 2.4.2. The gate electrode is simplified as an ohmic contact for cations, i.e. it is assumed that any redox reaction at the gate is fast enough to retain the equilibrium concentration of cations at the interface. Source and drain electrodes are treated as ohmic contacts by setting the hole concentration at the interface to the doping concentration. For cations, source and drain are assumed to be ideally reflecting, forcing the ion currents at the contacts to zero.

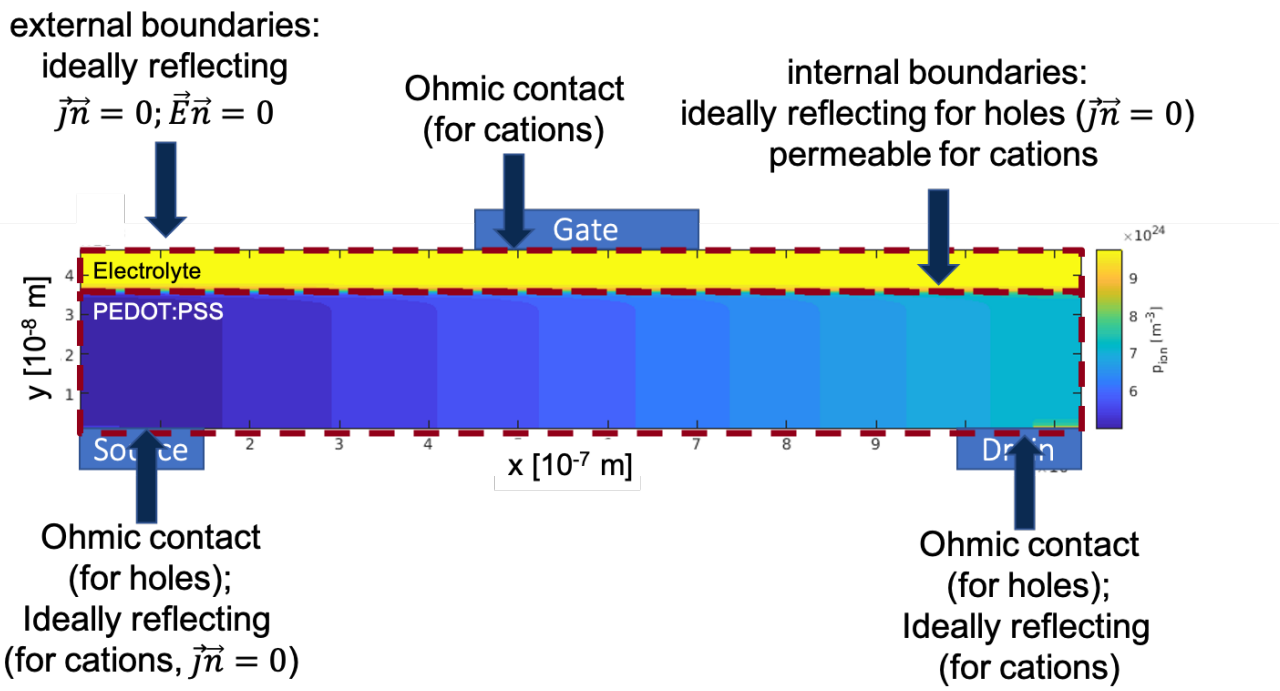

Figure 3: Setup of the numerical model used here[35]. The device consists of source, drain, and gate electrode, an electrolyte layer on top, and a semiconductor layer at the bottom. Reprinted with permission from[35].

Cations and holes in the PEDOT:PSS layer are assumed to co-exist in a single phase, i.e. details of the interpenetration network of a PEDOT and a PSS phase[42, 43] are not considered. Interaction between ions and holes are treated as purely electrostatic in nature as mediated by the right side of Poisson's equation.
To increase the stability of the numerical computation, all physical quantities are normalized, e.g. the applied voltages are normalized to the thermal voltage $V_T = \frac{k_B T}{e}$ (k_B: Boltzmann constant, T: temperature). In the following, the model is used to discuss experimental trends only. Although the model is capable to fit the results quantitatively as well[35], the uncertainty in the materials parameters would overemphasize the predictivity of the model.

2.2 General Switching Behavior

Figure 4 displays the general simulation protocol used here. An OECT with a channel length of $L = 1.13\mu m$ and organic semiconductor thickness of $T = 34nm$) is used as example. A square voltage pulse of $V_G = \pm 4V_T$ is applied to the gate electrode; the source potential is kept at $V_S = 0V$ and the drain at $V_D = -V_T$. The small drain potential ensures that the devices are studied in their linear regime.
Care is taken to let the simulation reach equilibrium before the next switching event. The simulation starts with the device in its equilibrium state at $V_{GS} = -4V_T$, i.e. the first half of the simulation time represents off switching, whereas the second half shows the trends during on-switching.
Figure 4 shows (from top to bottom) the applied gate voltage puls, the source current I_S, drain current I_D, and gate current I_G. Source and drain currents follow the same trends marked by an exponential relaxation toward the respective steady-state current. The gate current mirrors this behavior; it shows a short spike that exponentially decays to zero.
The currents shown in Figure 4 provide a macroscopic view of the OECT response only. To discuss microscopic details of the off- and on- switching process, two-dimensional plots of the cation concentration are shown in Figures 5 and 7. Figures 5 and 7 display snapshots at increasing times after the off and on switching event, respectively. Movies of the switching process displaying the evolution of the cation concentration, the electric potential, and the hole concentration are provided in the supplementary information.

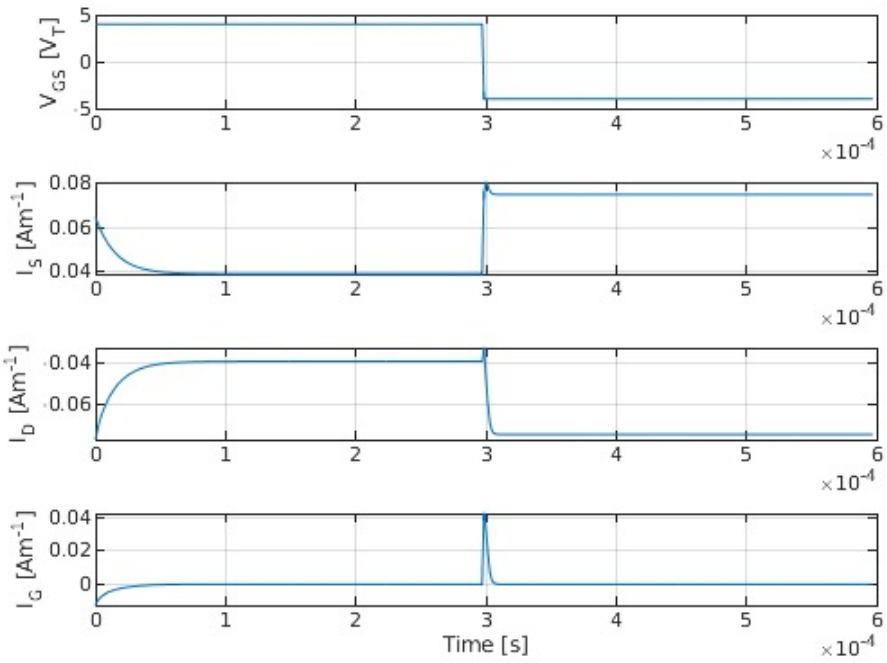

Figure 4: General simulation protocol applied here. Whereas the drain potential is kept constant (here: $V_{DS} = -1V_T$), a square voltage pulse $V_{GS}(t)$ is applied to the gate (here: $V_{GS} = \pm 4V_T$). The simulation starts with transistors that are in the steady state at negative voltages (here: the steady state at $V_{GS} = -4V_T$), so that the first half of the simulation corresponds to an injection of cations into the semiconductor and hence the off-switching process. In the middle of the simulation, the polarity of the gate voltage is reversed. Except for **Figure 16**, it is ensured that the transistor has reached steady conditions before any switching event.

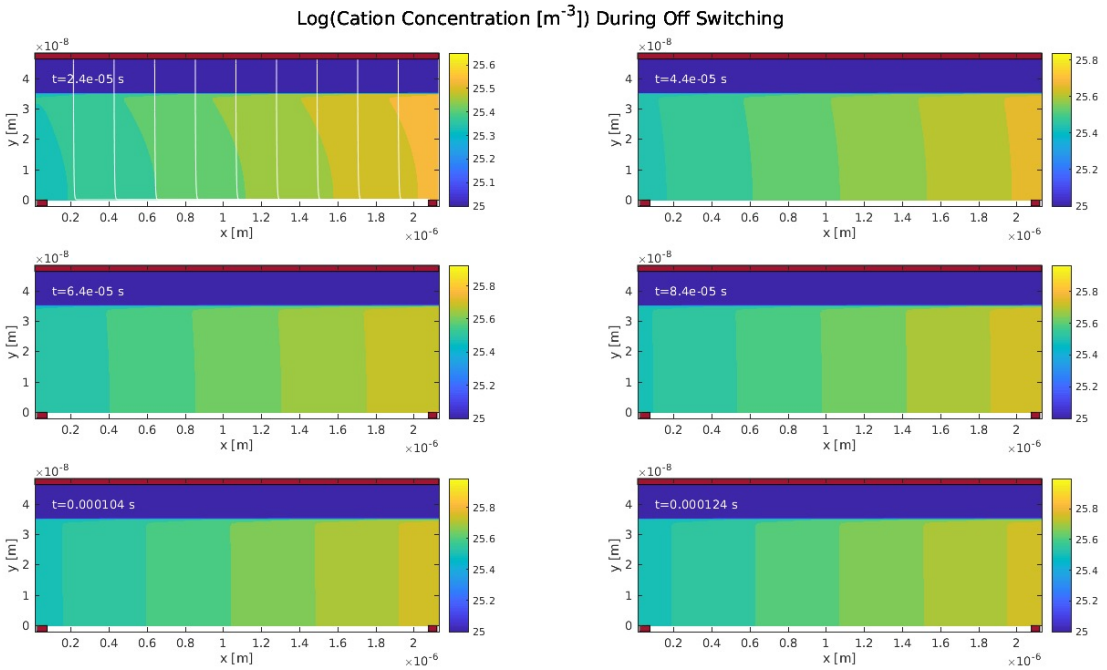

Figure 5: Snapshots of the distribution of cations during off-switching. The gate electrode is marked by a red box on top of the device, whereas source and drain electrodes are marked by small red boxes at the bottom left and right, respectively. The cation concentration in the electrolyte is almost constant (dark blue region), in contrast to the cation concentration within the PEDOT:PSS layer, which shows a strong gradient from source to drain electrode. The upper left panels includes white lines representing the direction of the flow of cations. The drain potential is kept at $V_{DS} = -1V_T$, and the gate potential is switched from $V_{GS} = -4V_T$ to $4V_T$.

Switching from the equilibrium state at $V_{GS} = -4V_T$ to $V_{GS} = 4V_T$ is shown in **Figure 5**. In this plot, the position of the gate electrode is marked by a thin red box at the top of the device; source and drain are indicated by smaller red boxes on the bottom left and right of the figures. The electrolyte is visible by the dark blue area of (almost) constant ion concentration, and the PEDOT:PSS layer below shows a gradient in ion concentration.
Overall, ions are injected homogeneously into the organic semiconductor along the whole device length. Already after $40 - 50\mu s$, the cation concentration along the y-axis is constant within the organic semiconductor ($\frac{dp_{ion}}{dy} \approx 0$), and a gradient in concentration along the x-axis is formed.
To visualize the flow of ions during switching, lines that symbolize the path of ions injected into the device at the gate are added to the upper left 2D plot. These streamlines indicate that ions are injected vertically into the organic layer, continue to flow vertically towards the bottom of the channel, where they turn and continue horizontally toward the drain electrode.
Whereas the streamlines only provide a qualitative understanding of the direction of the ion flow, vertical ($j_{ion,y}$) and horizontal ($j_{ion,x}$) components of the ion currents at the midpoint position between source and drain are displayed in **Figure 6**.
Figure 6 shows horizontal and vertical ion currents during a full switching cycle. The precise ratio between vertical and horizontal currents depends on the vertical position inside the organic semiconductor, plotted here is the current density at $y = 0.5nm$, i.e. close to the bottom of the device.
Figure 6 shows that ions are quickly injected into the organic layer by vertical currents, which leads to a rapid de-doping of the organic layer and consequently drop in drain current. However, these vertical currents quickly subside during off-switching. In contrast, the magnitude of lateral ion currents increases and reaches a maximum at approx. $t = 200 - 300\mu s$. Following this maximum, lateral currents drop to zero slowly, and steady-state is finally reached. Therefore, although the drain current is expected to drop quickly due to a rapid de-doping by vertical ion currents, the overall time to reach steady state is domi-

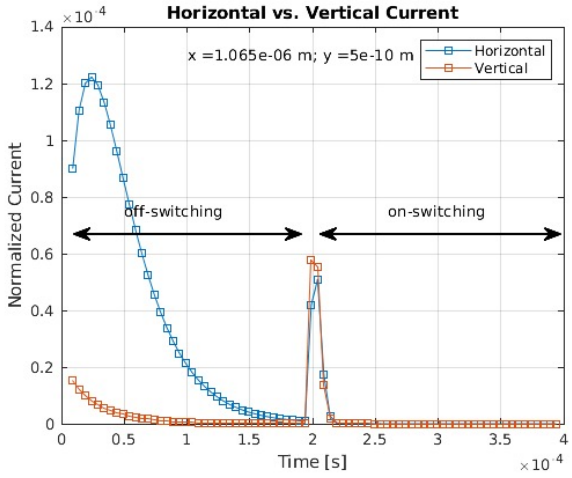

Figure 6: Horizontal ($j_{ion,x}$, blue) vs. vertical ($j_{ion,y}$, red) ion currents at the middle of the transistor channel during off- and on- switching. Whereas horizontal currents dominate during off-switching, they are less dominant during on-switching.

nated by lateral ion currents needed to reach the equilibrium concentration of ions along the channel. The cation distribution during on-switching is shown in **Figure 7**. In contrast to off-switching, on-switching is not homogeneous along the transistor channel.
As the ion concentration is highest at the drain, most ion currents originate there. The streamlines of ions starting at the drain electrode are shown in the upper left plot. In contrast to off-switching, these ions do not flow laterally along the transistor channel, but are oriented upward and are quickly drained at the gate electrode.
This difference between the ratio of lateral and vertical ion currents is seen as well in Figure 6. In contrast to off-switching, horizontal and vertical currents are on the same order of magnitude, which is in line with the tendency of cations to drain quickly towards the top of the OECT.

2.3 Scaling of Switching

The previous analysis has shown that switching of OECTs deviates significantly from previous models used to discuss OECTs. In particular, the use of an average ion and hole concentration along the transistor channel hides effects of lateral ion currents, which were shown to strongly influence off switching. To see if these differences have an impact on the switching times and scaling laws of OECTs, the response of OECTs with varying PEDOT:PSS layer thicknesses T, channel lengths L, and ion mobility μ (connected to the diffusion constant D via Einstein's equation) are shown in **Figure 8**.

2.3.1 Thickness Scaling

The transient response of the drain current for varying thickness of the PEDOT:PSS layer ($T = 17, 34, 51, 68, 85nm$) is shown in Figure 8, top. For all cases, the drain current follows a simple exponential relaxation in response to a voltage step applied at the gate electrode. As seen as well, the steady state current reached after longer simulation times scales with the thickness of the organic layers, which is in agreement with known steady-state scaling laws of OECTs[41].
The characteristic time constant of this exponential rise/decay of the drain current during off-switching τ_{off} (i.e. for $0 < t < 300\mu s$) and on-switching τ_{on} (for $300\mu s < t < 600\mu s$) calculated as the time taken until the current drops to $1/e$ of its initial value, is plotted vs. the channel thickness in **Figure 9a** and **Figure 9b**. Both time constants increase almost linearly with the organic layer thickness. This direct proportionality between the characteristic time of switching and thickness T can be explained with the help of **Figure 9c**, which plots the total ionic charge injected into the organic layer, calculated by integrating the gate current over time. Overall, the total ionic charge injected scales linearly with the

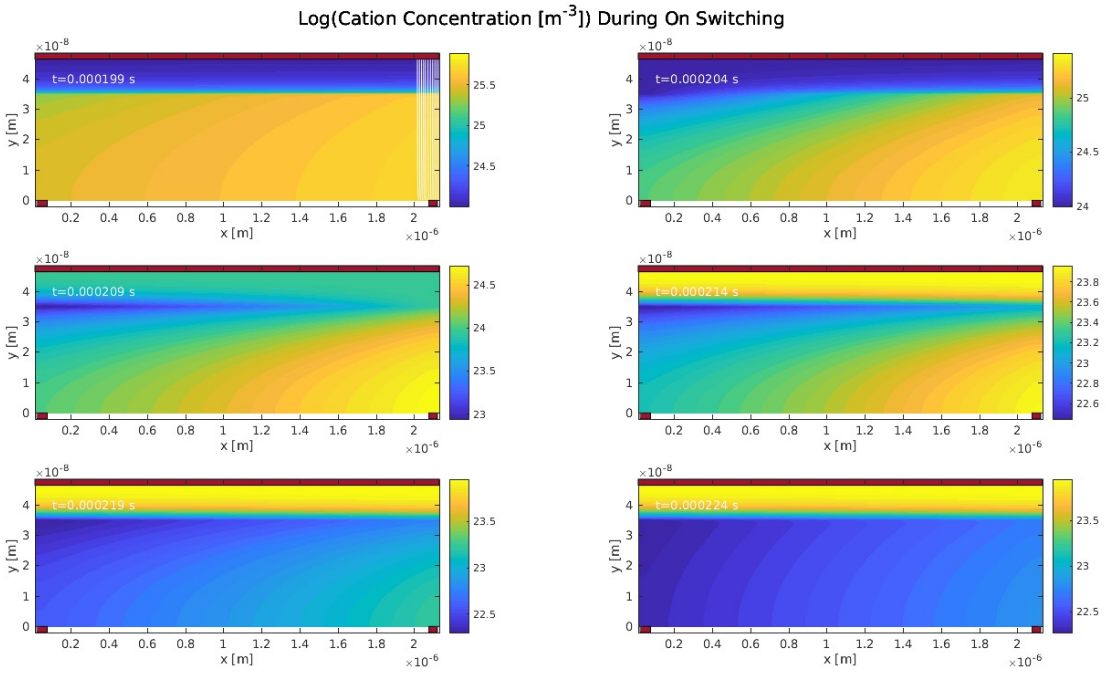

Figure 7: Snapshots of the cation distribution during on-switching. Ions originating from the drain are extracted rapidly at the gate electrode, leading to stronger vertical currents compared to off-switching. Please note that the scale was adjusted between different time steps to show the changes in the ion concentration inside the organic layers.

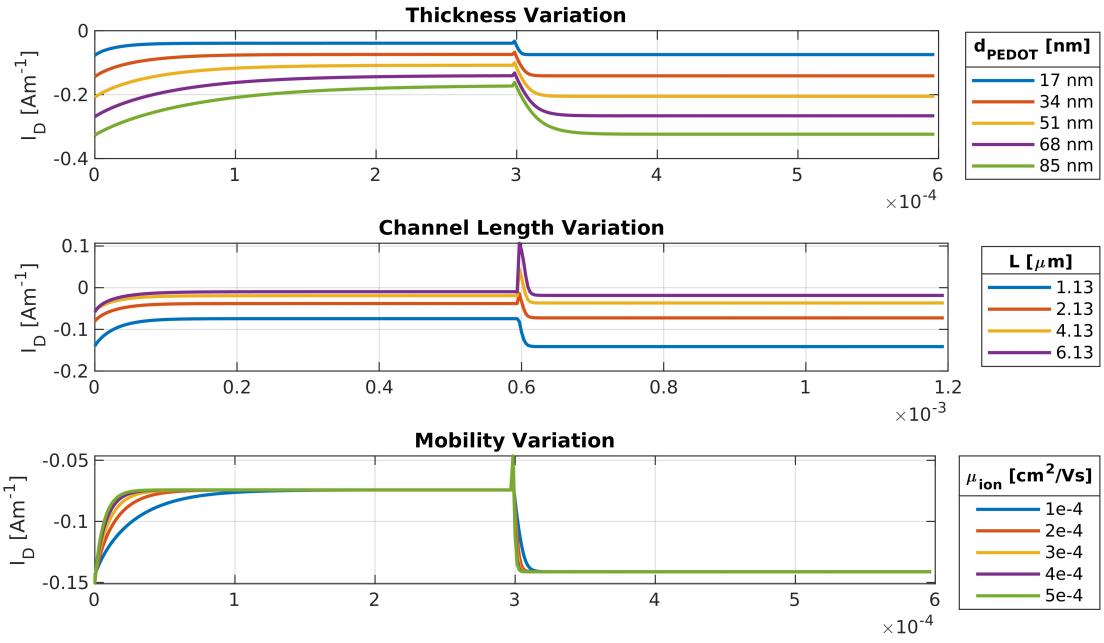

Figure 8: Scaling of the transient response of OECTs with the thickness of the organic layer (top), the channel length (middle), and the ion mobility (bottom)

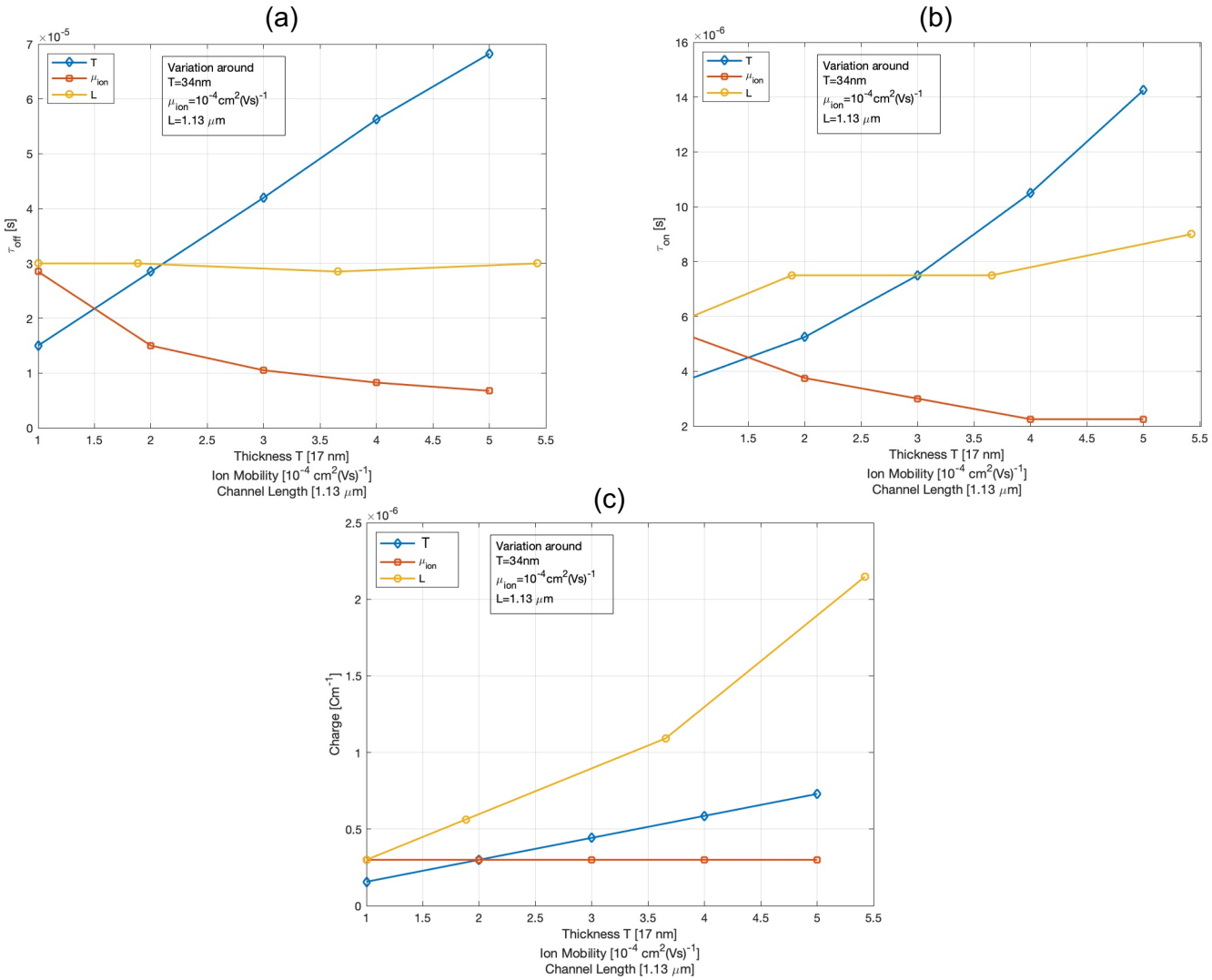

Figure 9: Scaling of the characteristic time constant of off-switching (τ_{off}, a), the time constant of on-switching (τ_{on}, b), and the total ionic charge injected into the semiconductor (c).

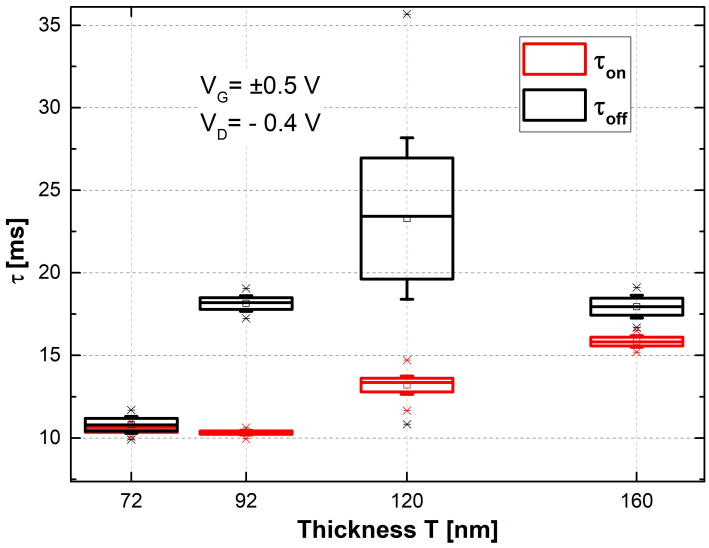

Figure 10: Time constants τ_{on} and τ_{off} vs. thickness of the organic semiconductor T (channel width $w = 2\ mm$, channel length $L = 350\ \mu m$) measured at $V_{DS} = -0.4V$.

thickness T. As all other geometric dimensions, in particular the channel length and the thickness of the electrolyte, are kept constant, it takes longer to charge thicker organic layers.
The predicted dependency of τ_{on} and τ_{off} on the thickness of the PEDOT:PSS layer can be confirmed by experiments. **Figure 10** plots both time constants vs. the organic layer thickness measured at a constant drain potential of $V_{DS} = -0.1V$ (channel length $L = 350\mu m$ and width $w = 2mm$). A symmetric square wave of $V_{GS} = \pm 0.5V$ is applied to the gate electrode. A relatively low frequency of $f = 1.5Hz$ is used to ensure that the transistors reach steady state before the next switching event. The square symbols represents mean time constants, the box size indicates the standard error, and stars denote outliers. The data was calculated from a set of at least 4 transistors and 12 measurements for each data point. As expected from the model, the devices show an increase in their time constants for thicker PEDOT:PSS films, confirming the bulk nature of the switching mechanism of OECTs.
A comparison of the simulated time constants τ_{on} and τ_{off} (Figure 9 a) and b)) shows that on-switching is consistently faster than off-switching. This difference can be explained by the different contributions of lateral ion currents to the different switching events, as discussed above. During off-switching, ions are homogeneously injected into the PEDOT:PSS layer, and transported laterally toward the drain electrode. During on-switching, in contrast, ions are moving predominantly vertically from the transistor channel toward the gate. Considering that the channel length of OECTs is usually much larger than the thickness of the semiconductor layer, lateral ion currents limit off-switching events and render them slower than on-switching.
Although the time constants extracted from the experiment tend to show the same trends (cf. Figure 10), i.e. a slower off-switching and faster on-switching is observed, the difference between τ_{off} and τ_{on} is smaller than expected from the simulation. This difference might be caused by defects in the materials not included in the model, or the significantly larger distance of the gate electrode from the transistor channel in the experiment compared to the rather thin electrolyte layer used in the simulation. This larger distance leads to an increased ionic resistance, which reduces direct vertical ion currents and hence diminishes the difference between the magnitude of lateral and vertical ion currents in real devices.
Furthermore, in addition to the effect of different migration pathways taken by the cations during off- and on-switching, a difference in conversion rates between neutral, polaronic, and bipolaronic species on PEDOT:PSS during doping and de-doping as found by Paulsen et al.[44] and Rebetez et al.[45] can contribute to asymmetry seen between on and off switching. Adding detailed reaction kinetics of the doping and de-doping process will help to distinguish between these effects in the future.

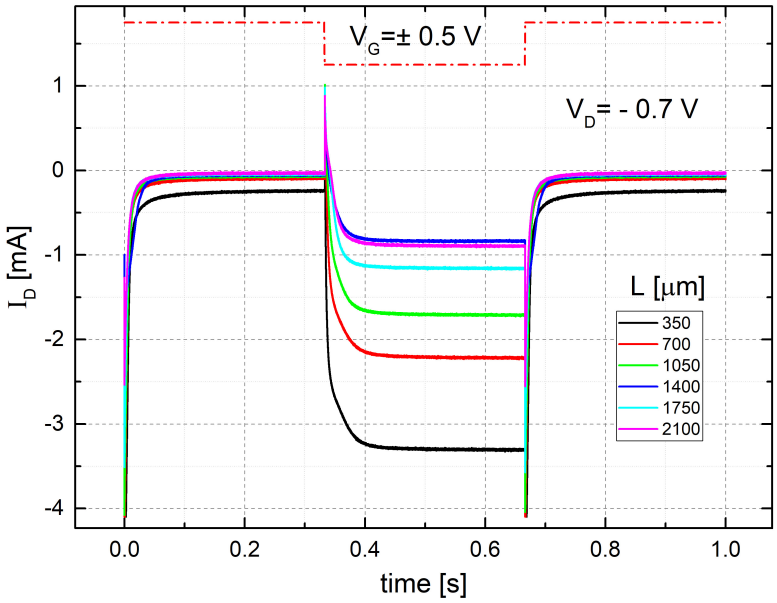

Figure 11: Drain currents in response to square wave gate signals ($V_G = \pm 0.5V$). Dimensions of the channel are $L = 350\mu m$, $w = 2mm$, $T = 160nm$. All transistors show a spike and recovery pattern as described by Bernards model.

2.3.2 Channel Length and Mobility Scaling

The middle panel of Figure 8 plots the response of transistors with increasing channel length to symmetric square waves applied to the gate. In contrast to the thickness dependency, the characteristic shape of the switching process changes. Starting from a continuous relaxation for the shortest channel ($L = 1.13\mu m$), the response changes into an increasingly spiking one for longer channel lengths L. Furthermore, as expected from Equation 4 and steady state simulations as well[35, 41], the steady state current $I_{D,ss}$ is inversely proportional to the channel length L.
The characteristic time constants for on-switching τ_{on} shown in Figure 9 is still smaller than the one for off switching τ_{off} for all channel lengths, reflecting the same trend as seen above. However, in contrast to increasing the thickness T, an increase in channel length L does not increase these time constants. Although increasing the channel length increases the overall volume of the organic layer and amount of injected cations into the organic semiconductor (cf. Figure 9c), the total ionic resistance R_i of the electrolyte decreases inversely proportional to the channel length. Hence, the increase in total ionic charge cancels with an increase in gate currents. However, it has to be stressed that this analysis neglects any parasitic series resistances, i.e. cable resistances or limited driving currents from a previous stage in a logic circuit, which could add additional limitations to the transient response at larger channel lengths. Again, the trends seen in the simulation can be reproduced in experiments. **Figure 11** plots the full response of transistors with varying channel length ($L = 350$, 700, 1050, 1400, 1750, 2100 μm) to a square input voltage wave of $V_{GS} = \pm 0.5V$ at different drain potentials V_{DS}. For the channel lengths studied here, OECTs always show a spiking response. Furthermore, the steady state current clearly scales with the inverse of the channel length.
Time constants extracted from the experiments are shown in **Figure 12**. Time constants were measured for a wider range of drain and gate potentials, and show no (τ_{on}) or only weak (τ_{off}) dependency on the channel length. The slight increase in (τ_{off} with channel length could be caused by parasitic resistances of the measurement setup, increasing the time constant.
Finally, the bottom panel of Figure 8 and Figure 9 plot the dependency of switching on the ion mobility. As expected, the increase in ion mobility does not influence the amount of ionic charge injected into the organic semiconductor. However, lateral and vertical ion currents inside the organic layer increase for larger mobilities, and the devices responds faster to the voltage step. Consequently, both, on and off switching time constants decrease for larger ion mobilities.

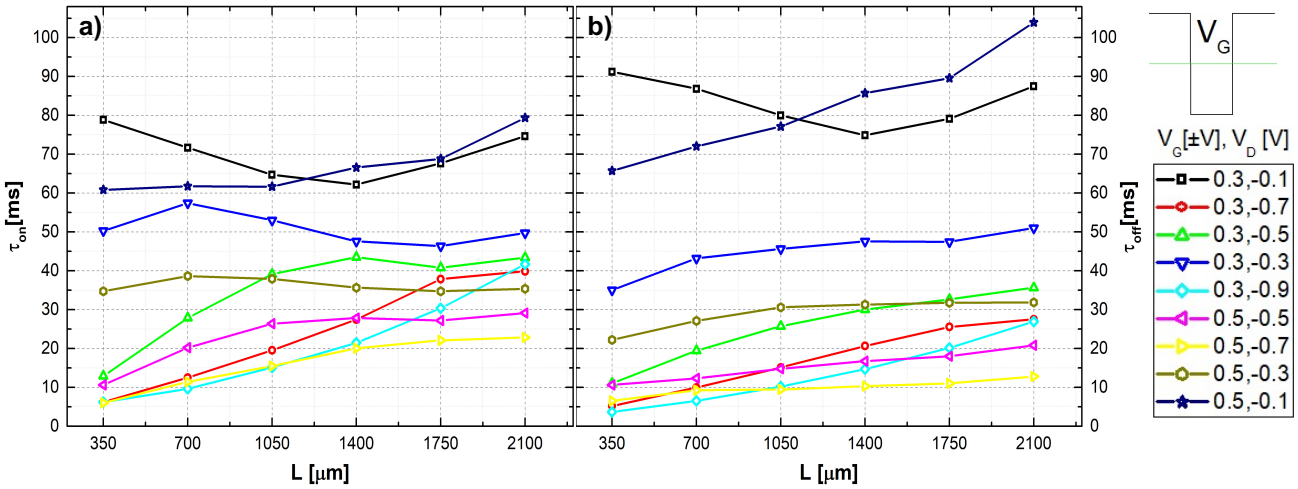

Figure 12: Dependency of time constants τ_{on} (a) and τ_{off} (b) on the channel length. No systematic dependency is found for a wide range of applied drain and gate potentials. Dimensions of channel are $w,\ d = 2\ mm,\ 160\ nm$

2.3.3 Comparison of Trends with Predictions from Bernard's model

The scaling trends shown here are in line with the trends predicted by Bernard's model (Equation 7). For example, the thickness dependency can be explained assuming that the system is limited by the charging of the organic layer with ions. Hence, the ionic time constant $\tau_i = R_s C_G$ determines the response. As the gate capacitance is found to scale with the volume of the organic semiconducting layer, a proportionality of $\tau \propto d$ is indeed expected.
Similarly, the transition from a simple relaxation in drain current to an increasingly spiking type response is in line with the discussion of Figure 2, where it was shown that the response of OECTs is expected to be a simple relaxation behavior if $f\frac{\tau_e}{\tau_i} \ll 1$. However, as $\tau_e = \frac{L^2}{V_D \mu}$ scales with the square of the channel length, a transition to a spiking response for $\tau_e \approx \tau_i$ is anticipated for devices with longer channels.
Although Bernard's model seems to describe the thickness, mobility, and channel length dependency well, it cannot describe the full switching process and fails to correctly describe other trends. The first example is the apparent asymmetry between on and off switching, which was consistently observed in all simulations. More cases, where a full 2D device simulation is needed to describe the OECT correctly, are discussed in the following.

2.4 Influence of Lateral Ion Currents on Switching

As discussed above, off-switching of OECT is characterized by a rapid charging of the organic layer with cations, driven by vertical ion currents, and a subsequent re-distribution of cations along the transistor channel due to lateral currents. These lateral currents are essential to reach the equilibrium state of the OECT, and to establish an accumulation of cations at the drain [35].

2.4.1 Influence of the Drain Potential V_{DS}

Lateral ion currents are driven by the lateral electric field created by the potential difference between the source and drain electrode V_{DS}. Therefore, it is expected that the magnitude of lateral currents and in turn the time constant of off-switching depends on the drain potential.
Figure 13a plots the simulated lateral and vertical ion currents, normalized to their maximum value, for different drain potentials. Indeed, increasing the drain potential results in a larger lateral field along the transistor channel, which in turn results in a faster relaxation and faster drop in lateral ion currents. Vertical currents, however, are only weakly influenced by the potential applied to the drain. Furthermore, ion currents during on-switching were observed to not be affected by the drain potential.

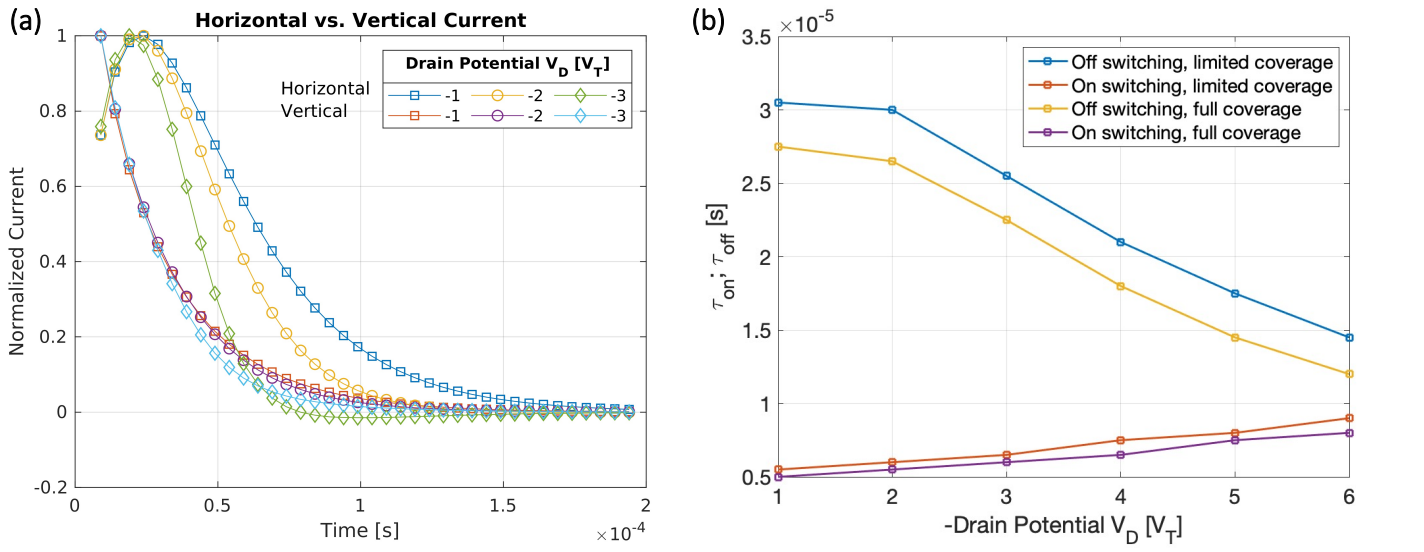

Figure 13: a) Dependency of horizontal and vertical ion currents $j_{ion,x}$ and $j_{ion,y}$ on the applied drain potential. Whereas vertical currents are only weakly influenced by the drain potential, horizontal currents drop faster for larger drain potentials. All curves are normalized to their maximum value. b) Characteristic time constants of off- and on-switching τ_{off} and τ_{on}. Whereas on-switching does not strongly depend on the drain potential, off-switching is considerably faster for higher negative drain potentials.

This dependency leads to time constants that depend on the applied drain potential (cf. **Figure 13b**). As expected from the trends in lateral and vertical ion currents, the off-switching time constant τ_{off} drops for larger (negative) drain potential, whereas the on-switching time constant remains fairly constant or even increases slightly.
The dependency of the switching time on the drain potential is seen in the experimental data shown in **Figure 14**, which plots τ_{on} and τ_{off} for transistors with different PEDOT:PSS thickness. For all variations, a clear drop in the switching times for larger negative drain potentials is observed.
Although a weaker influence of the drain potential on the on-switching time constant τ_{on} compared to the off-switching time constant is found in Figure 10, the drop in the on-switching times is in contrast to the simulation. As discussed above, this discrepancy can be explained by the larger ionic resistance of the electrolyte in the experiment, which reduces the influence of vertical ion currents during on-switching and hence amplifies the significance of the lateral drain potential.

2.4.2 Geometry dependency

Not only does the lateral ion current result in a drain potential dependence of the off-switching, it introduces as well a complex geometry dependence of the switching process not properly accounted for in previous models. To discuss this influence, the device model is altered so that the gate electrode of the OECT does not cover the complete device, but only a smaller portion of the OECT in the center of the transistor channel. Whereas this change does not influence the steady state of the device, it distinctly changes the transient response during switching.
The result of these simulations is shown in **Figure 15**, which plots the cation distribution inside the device after application of a positive potential to the gate. The shortened gate electrode is indicated by a small red rectangular on top of the device.
In contrast to the results obtained for a gate that extends across the complete device (Figure 5), cations are only injected underneath the gate electrode, i.e. in the middle of the transistor channel. From there, cations have to migrate laterally toward the drain or source electrode. This additional lateral current component needed to switch the transistor off leads to a slowing down of the transistor. In Figure 13b τ_{on} and τ_{off} are compared for the different gate electrode geometries. For all drain potentials, an increase in τ_{on} and τ_{off} is observed for smaller gate electrodes.

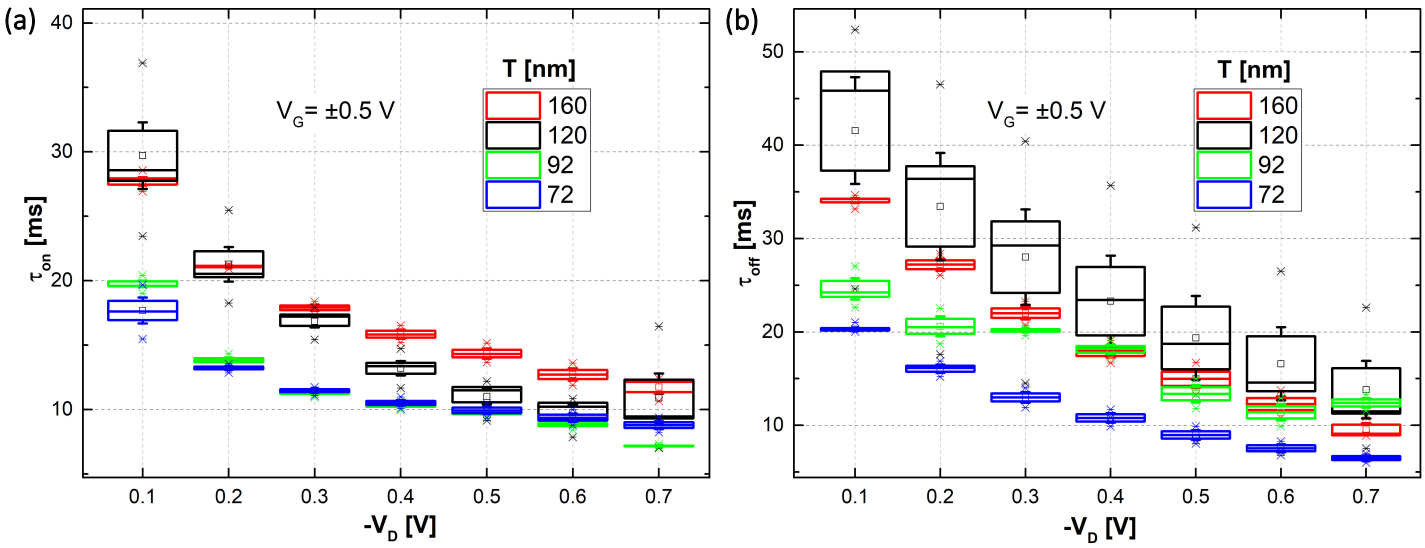

Figure 14: Scaling of the characteristic time constant for off-switching (τ_{off}, a), the time constant for on-switching (τ_{on}, b) with the applied drain potential V_D.

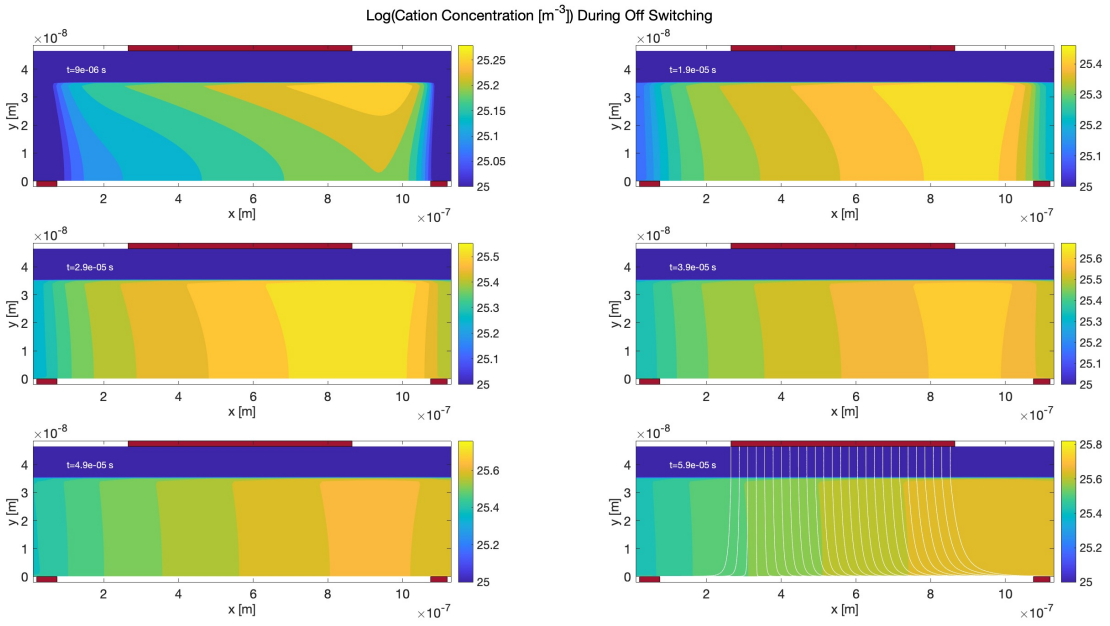

Figure 15: Snapshots of the cation distribution during off-switching. In contrast to Figure 5, the gate electrode is not extending across the whole device. That leads to a slow migration of ions toward the sides of the device.

2.4.3 Frequency dependence of Switching

During all model calculations and experiments discussed above, a low frequency of the square input pulse was used. Furthermore, steady-state conditions were enforced in the model before the gate voltage changes polarity to ensure that the true time constants are extracted from the current transients.
This additional precaution was not taken in **Figure 16** and the frequency of the input pulse was increased from $f = 2.5kHz$ to $80kHz$. The resulting current transients and the applied voltage waveforms are displayed in **Figure 16a**. For increased frequencies, the device is not fully switched off during the first half of the cycle duration, i.e. the drain current does not reach its equilibrium value.
In contrast to off-switching, steady state conditions are reached after on switching for all frequencies. As seen in Figure 16b, devices relax faster towards this steady state at higher frequencies, resulting in an seemingly shorter time constant. However, this reduction in switching time is not due to an increase in device performance, but due to an insufficient off-switching process preceding the negative gate voltage pulse. This is illustrated in Figure 16c. For higher frequencies, less ionic charge is injected into the organic layer, which corresponds to the incomplete off-switching observed in Figure 16a. Hence, during the subsequent on-switching event, less ions have to be removed from the semiconductor, leading to an incorrect calculation of the on switching time τ_{on}.
This apparent dependency of the switching time constants on frequency can be reproduced in the experiments, which is shown in Figure 17. Again, a square voltage pulse is applied to the gate, but the frequency of switching is increased from 0.1 to $100Hz$. For the highest frequency, the transient response doesn't reach steady state conditions (Figure 17 a), leading to a drop in the on and off current I_{ON} and I_{OFF} shown in Figure 17 b). Most importantly, the apparent switching time constants, shown in Figure 17c drop with frequency, already before the decrease in the on and off current becomes noticeable.
Overall, these results show that care has to be taken when characterizing the transient response of OECTs. Not only has to be ensured that devices reach steady state conditions after the switching event, but before as well. Otherwise, artificially short time constants and consequently high switching frequencies can be deduced that are not representative of the device performance.

3 Discussion and Conclusions

Although Organic Electrochemical Transistors rely on a slow migration of ions, they have been reported to be able to switch quickly, which reinforces their status as one of the most promising device technology for organic biosensing.
Current device models used to discuss OECT switching approximate the ion and hole concentration along the transistor channel with their average value, which reduces this complex problem into a one dimensional one that can be solved analytically. As shown here as well, these models are successful and can correctly reproduce scaling trends for the thickness of the organic layer, the channel length, or the ion mobility.
However, averaging hole and ion concentrations along the transistor channel neglects lateral ion currents flowing inside the transistor channel. Here, it is shown that these lateral currents can limit the switching process. Following a rapid drop in drain current, caused by ions vertically injected into the transistor channel, ions re-distribute inside the channel by lateral currents until the steady state of the OECT is reached. Depending on the applied drain potential, channel length, and precise geometry of the OECT, this second step can be slow and is seen by a slow relaxation of drain currents.
These results have a significance for reporting on response times of OECTs. Response times have to be interpreted in relation to the applied drain potential, as a larger drain voltage can lead to a faster response despite using a semiconductor material with lower ion and charge mobility. Similarly, care has to be taken to characterize the full swing of the transistor between the two steady-state conditions at the gate voltages before and after application of the voltage pulse. Although fast response times can be reached, these values do not necessarily represent the full swing of the transistor and might merely represent switching between two transient states.

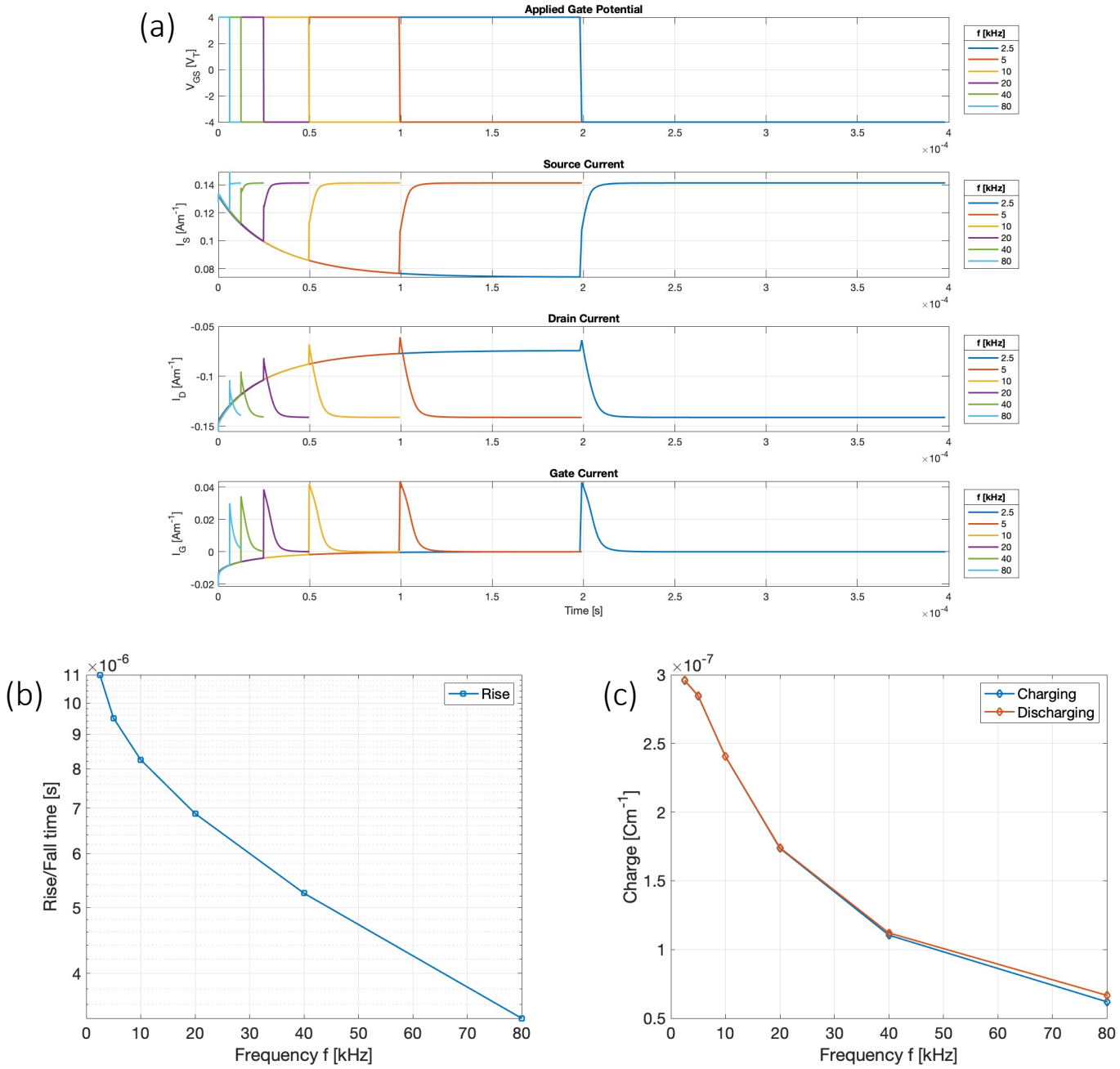

Figure 16: Dependency of the measured time constants on the frequency of the applied gate pulse. (a) Applied gate voltage pulses and simulated source, drain, and gate currents. (b) Dependency of the rise time calculated from the simulation results on the frequency. (b) Amount of charge injected or removed during the switching cycle.

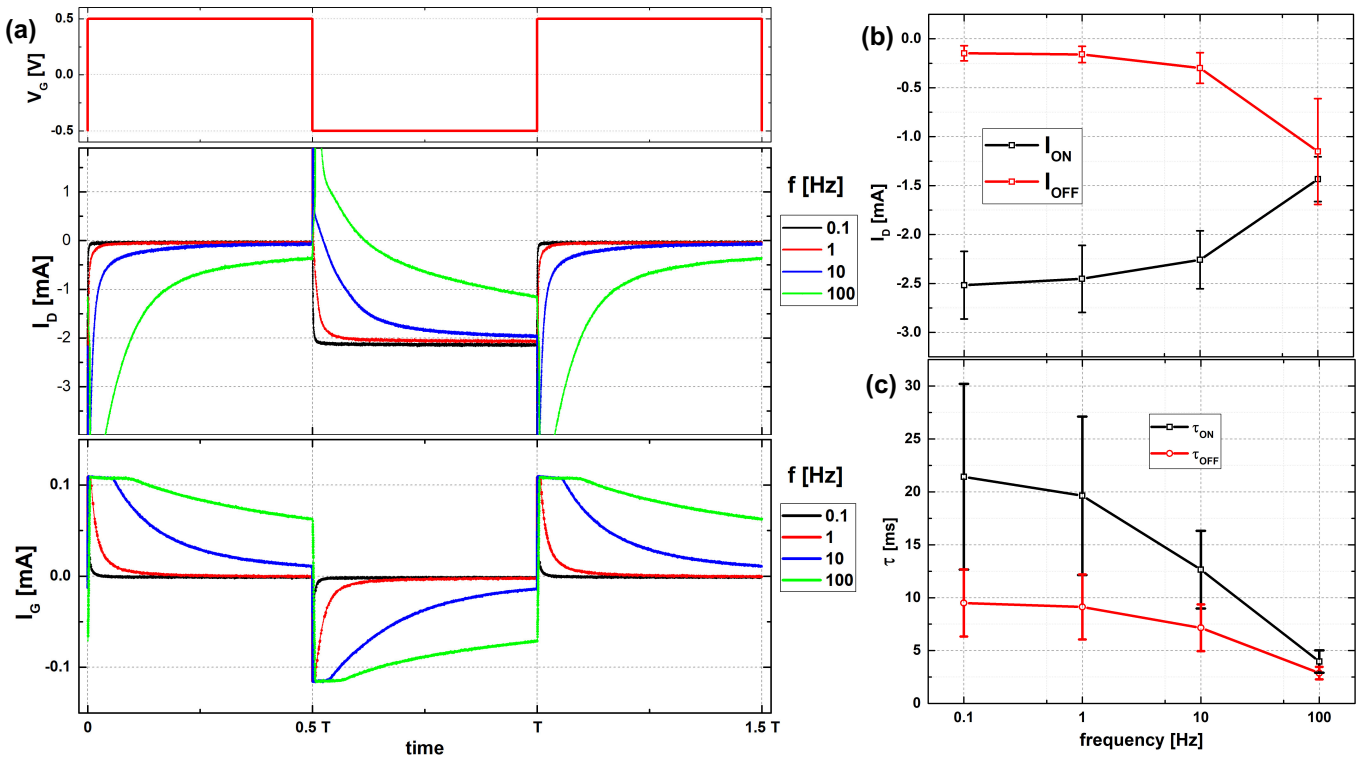

Figure 17: Frequency dependence of the transient response of OECTs. (a) Applied gate voltage pulses and resulting drain and gate currents. The gate current was limited to $\sim \pm 0.1\ mA$. (b) Drain current in the ON and OFF states at varying frequencies. (c) τ_{on} and τ_{off} in dependence of the frequency of the applied gate signal. A symmetric square gate signal of $\pm 0.5\ V$ was used and the drain was maintained at $-0.4\ V$ with respect to the source. Each data point is an average of 8 OECTs. Dimensions of the channel are $L,\ w,\ T = 350\ \mu m,\ 2\ mm,\ 160\ nm$.

4 Experimental Details

OECT devices were processed on 21.5 mm × 21.5 mm × 1 mm plain glass substrates. Precisely cut glass substrates are cleaned in a clean-room facility using a standard protocol. Substrates are first sonicated for 25 minutes followed by thorough rinsing with lab grade organic solvents (isopropyl alcohol, methanol and acetone) and subsequent drying. Cleaning is followed by deposition of 15 nm chromium and 40 nm gold metals to form source and drain electrodes. Thermal evaporation using the EvoVac system of Angstrom Engineering at a rate of 0.4 $\mathring{A}s^{-1}$ was used. The background pressure in the system remained below 10^{-6} Torr. These electrodes were structured using shadow masks during deposition. The width of the channel varied from $350 - 2100\ \mu m$, the channel width was fixed to 2 mm.
To deposit the PEDOT:PSS layer, 10 ml of PH 1000 solution from Clevios was mixed with 0.5 ml ethylene glycol (EG) and 25 μl dodecyl benzene sulfonic acid (DBSA) to enhance the conductivity of the semiconductor. A small amount ($1\%w/w$) of (3-Glycidyloxypropyl)trimethoxysilane (GOPS) was also added to increase adhesion and strength of the PEDOT:PSS film. This PEDOT:PSS solution was spin-coated on the substrates using the spin coater "P6204-A" of Specialty Coating Systems at variable speeds (1000-5000 rpm) for a minute, leading to thickness varying from $\sim 72 - 160\ nm$.
Spin coating was followed by an hour-long baking on a hot plate at $140°C$. The PEDOT:PSS polymer film was structured using oxygen plasma and glass masks in a oxygen plasma (200 W for 5 min, Oxford 80 Plasma Lab). 100 mM NaCl solution in DI water was used as electrolyte. EG, DBSA, GOPS, and NaCl were purchased from Sigma-Aldrich and used as received. To confine the electrolyte, a well of Polydimethylsiloxane (PDMS, DOW Sylgard 184 silicone elastomer kit and curing agent) was used. A silver rod was used as the gate electrode. All transient characterization was done using a Tektronix 4 Series Mixed Signal Oscilloscope (TEK MSO46) and an in-house built operational amplifier to reduce noise. All voltages were referenced to the source electrode kept at ground.

Supporting Information

Supporting Information is available from the Wiley Online Library or from the author.

Acknowledgements
Part of device fabrication was done at the Prototype Facility of the Advanced Material and Liquid Crystal Institute, Kent State University. The authors gratefully acknowledge funding from the National Science Foundation (Grant ECCS 1750011 and ECCS 1709479).
Data Availability Statement The data that support the findings of this study are available from the corresponding author upon reasonable request.

References

[1] B. D. Paulsen, K. Tybrandt, E. Stavrinidou, J. Rivnay, *Nature Materials* **2020**, *19*, 1 13.

[2] D. Khodagholy, J. Rivnay, M. Sessolo, M. Gurfinkel, P. Leleux, L. H. Jimison, E. Stavrinidou, T. Herve, S. Sanaur, R. M. Owens, et al., *Nature Communications* **2013**, *4*, 1 2133.

[3] D. Khodagholy, T. Doublet, P. Quilichini, M. Gurfinkel, P. Leleux, A. Ghestem, E. Ismailova, T. Hervé, S. Sanaur, C. Bernard, et al., *Nature Communications* **2013**, *4* 1575.

[4] L. J. Currano, F. C. Sage, M. Hagedon, L. Hamilton, J. Patrone, K. Gerasopoulos, *Scientific Reports* **2018**, *8* 15890.

[5] L. Kergoat, B. Piro, D. T. Simon, M.-C. Pham, V. Noel, M. Berggren, *Advanced Materials* **2014**, *26*, 32 5658.

[6] C. Liao, M. Zhang, L. Niu, Z. Zheng, F. Yan, *Journal of Materials Chemistry B* **2014**, *2*, 2 191.

[7] Z. Zhu, J. Mabeck, C. Zhu, N. Cady, C. Batt, G. Malliaras, *Chemical Communications* **2004**, , 13 1556.

[8] S. Zhang, E. Hubis, G. Tomasello, G. Soliveri, P. Kumar, F. Cicoira, *Chemistry of Materials* **2017**, *29*, 7 3126.

[9] J. Ko, X. Wu, A. Surendran, B. T. Muhammad, W. L. Leong, *ACS Applied Materials & Interfaces* **2020**, *12*, 30 33979.

[10] S. Zhang, F. Cicoira, *Advanced Materials* **2017**, *29*, 40 1703098.

[11] J. Rivnay, R. M. Owens, G. G. Malliaras, *Chemistry of Materials* **2014**, *26*, 1 679.

[12] E. Likhtik, J. P. Johansen, *Nature Neuroscience* **2019**, *22*, 10 1586.

[13] T. Rothlander, P. C. Hutter, E. Renner, H. Gold, A. Haase, B. Stadlober, *IEEE Transactions on Electron Devices* **2014**, *61*, 5 1515.

[14] D. Khodagholy, M. Gurfinkel, E. Stavrinidou, P. Leleux, T. Herve, S. Sanaur, G. G. Malliaras, *Applied Physics Letters* **2011**, *99*, 16 163304.

[15] P.-O. Svensson, D. Nilsson, R. Forchheimer, M. Berggren, *Applied Physics Letters* **2008**, *93*, 20 415.

[16] A. Campana, T. Cramer, D. T. Simon, M. Berggren, F. Biscarini, *Advanced Materials* **2014**, *26*, 23 3874.

[17] J. Rivnay, P. Leleux, M. Ferro, M. Sessolo, A. Williamson, D. A. Koutsouras, D. Khodagholy, M. Ramuz, X. Strakosas, R. M. Owens, C. Benar, J.-M. Badier, C. Bernard, G. G. Malliaras, *Science Advances* **2015**, *1*, 4 e1400251.

[18] J. T. Mabeck, J. A. DeFranco, D. A. Bernards, G. G. Malliaras, S. Hocdé, C. J. Chase, *Applied Physics Letters* **2005**, *87*, 1 013503.

[19] P. C. Hütter, T. Rothländer, A. Haase, G. Trimmel, B. Stadlober, *Applied Physics Letters* **2013**, *103* 043308.

[20] H. Toss, C. Suspene, B. Piro, A. Yassar, X. Crispin, L. Kergoat, M.-C. Pham, M. Berggren, *Organic Electronics* **2014**, *15*, 10 2420.

[21] A. Savva, C. Cendra, A. Giugni, B. Torre, J. Surgailis, D. Ohayon, A. Giovannitti, I. McCulloch, E. Di Fabrizio, A. Salleo, et al., *Chemistry of Materials* **2019**, *31*, 3 927.

[22] A. Savva, R. Hallani, C. Cendra, J. Surgailis, T. C. Hidalgo, S. Wustoni, R. Sheelamanthula, X. Chen, M. Kirkus, A. Giovannitti, et al., *Advanced Functional Materials* **2020**, *30*, 11 1907657.

[23] H. Jia, Z. Huang, P. Li, S. Zhang, Y. Wang, J.-Y. Wang, X. Gu, T. Lei, *Journal of Materials Chemistry C* **2021**, *9*, 14 4927.

[24] A. G. Polyravas, V. F. Curto, N. Schaefer, A. B. Calia, A. Guimera-Brunet, J. A. Garrido, G. G. Malliaras, *Flexible and Printed Electronics* **2019**, *4*, 4 044003.

[25] P. Fromherz, W. Bainbridge, M. Roco, *Annals of the New York Academy of Sciences* **2006**, *1093* 143.

[26] D. A. Koutsouras, P. Gkoupidenis, C. Stolz, V. Subramanian, G. G. Malliaras, D. C. Martin, *ChemElectroChem* **2017**, *4*, 9 2321.

[27] P. A. Ersman, D. Nilsson, J. Kawahara, G. Gustafsson, M. Berggren, *Organic Electronics* **2013**, *14*, 5 1276.

[28] G. D. Spyropoulos, J. N. Gelinas, D. Khodagholy, *Science Advances* **2019**, *5*, 2 eaau7378.

[29] C. Cea, G. D. Spyropoulos, P. Jastrzebska-Perfect, J. J. Ferrero, J. N. Gelinas, D. Khodagholy, *Nature materials* **2020**, *19*, 6 679.

[30] J. Isaksson, C. Tengstedt, M. Fahlman, N. Robinson, M. Berggren, *Advanced Materials* **2004**, *16*, 4 316.

[31] H. Tang, P. Kumar, S. Zhang, Z. Yi, G. D. Crescenzo, C. Santato, F. Soavi, F. Cicoira, *ACS Applied Materials & Interfaces* **2015**, *7*, 1 969.

[32] G. Tarabella, G. Nanda, M. Villani, N. Coppede, R. Mosca, G. G. Malliaras, C. Santato, S. Iannotta, F. Cicoira, *Chemical Science* **2012**, *3*, 12 3432.

[33] P. R. Paudel, J. Tropp, V. Kaphle, J. D. Azoulay, B. Lüssem, *Journal of Materials Chemistry C* **2021**, *9* 9761.

[34] D. A. Bernards, G. G. Malliaras, *Advanced Functional Materials* **2007**, *17*, 17 3538.

[35] V. Kaphle, P. R. Paudel, D. Dahal, R. K. Radha Krishnan, B. Lüssem, *Nature Communications* **2020**, *11*, 1 2515.

[36] G. C. Faria, D. T. Duong, A. Salleo, *Organic Electronics* **2017**, *45* 215.

[37] G. C. Faria, D. T. Duong, A. Salleo, C. A. Polyzoidis, S. Logothetidis, J. Rivnay, R. Owens, G. G. Malliaras, *MRS Communications* **2014**, *4*, 4 189.

[38] J. T. Friedlein, M. J. Donahue, S. E. Shaheen, G. G. Malliaras, R. R. McLeod, *Advanced Materials* **2016**, *28*, 38 8398.

[39] N. Coppede, M. Villani, F. Gentile, *Scientific Reports* **2014**, *4* 4297.

[40] F. Gentile, D. Delmonte, M. Solzi, M. Villani, S. Iannotta, A. Zappettini, N. Coppede, *Organic Electronics* **2016**, *35* 59.

[41] P. R. Paudel, V. Kaphle, D. Dahal, R. K. Radha Krishnan, B. Lüssem, *Advanced Functional Materials* **2021**, *31*, 3 2004939.

[42] K. Tybrandt, I. V. Zozoulenko, M. Berggren, *Science Advances* **2017**, *3*, 12 eaao3659.

[43] A. V. Volkov, K. Wijeratne, E. Mitraka, U. Ail, D. Zhao, K. Tybrandt, J. W. Andreasen, M. Berggren, X. Crispin, I. V. Zozoulenko, *Advanced Functional Materials* **2017**, *27*, 28 1700329.

[44] B. D. Paulsen, R. Wu, C. J. Takacs, H.-G. Steinruck, J. Strzalka, Q. Zhang, M. F. Toney, J. Rivnay, *Advanced Materials* **2020**, *32*, 40 2003404.

[45] G. Rebetez, O. Bardagot, J. Affolter, J. Rehault, N. Banerji, *Advanced Functional Materials* **2021**, *32*, 5 2105821 .

Table of Contents

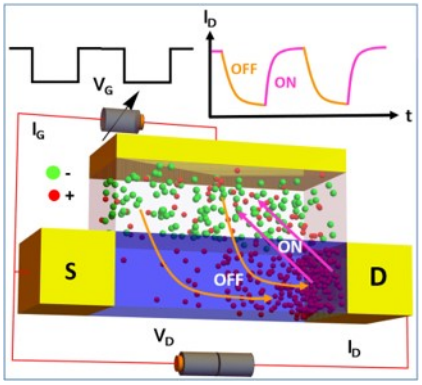

A fast response of Organic Electrochemical Transistors to changing environmental conditions is essential for their widespread use as sensors. Here, a 2-D drift-diffusion model is presented to gain a better understanding of transient processes limiting the speed of OECTs. It is shown that the switching is strongly influenced by lateral ion currents which in turn depends on the biasing conditions, and the detailed geometry.